computation of an accurate value.

Three of the compounds, namely PDG, PCPDG, and MCPDG, show a great sensitivity to ρ; their value of $\langle\mu^2\rangle$ decreases with increasing ρ. This effect comes mainly from the racemic dyad which in the t0,t0 conformation exhibits a value of μ^2 much larger than any of the other three allowed conformations; as ρ increases, the incidence of t0,t0 grows smaller and consequently $\langle\mu^2\rangle$ shows a sharp decrease. In racemic OCPDG, however, μ^2 is largest for tπ,tπ, while the other three conformations have roughly the same value. To increase ρ means then to raise the stability of tπ,tπ which depends on ρ^2, but it also stabilizes t0,tπ and tπ,t0 that depend on ρ. The net effect is a small increase of $\langle\mu^2\rangle$ with increasing ρ.

The value of OCPDG is also very sensitive to the rotation, ψ, over the O–Ph bond with $\langle\mu^2\rangle$ increasing as ψ increases. The explanation is straightforward: when ψ = 0 (as shown in Figure 4), the μ_1 and μ_3 components of the dipole moment of the ester have almost opposite directions and, therefore, there is a strong cancellation between them. This cancellation becomes smaller as ψ departs from 0, and consequently $\langle\mu^2\rangle$ for the dymer increases with increasing ψ. However, in the case of MCPDG, $\langle\mu^2\rangle$ is practically independent of ψ. The reason is that in this molecule the allowed positions for that rotation are ψ and 180–ψ (besides their symmetrical $-\psi$ and 180+ψ). With $\psi \approx 60°$, there is a partial cancellation between μ_1 and μ_3', but there is also a reinforcement between these two components when the rotation is 180–ψ. To modify the value of ψ changes both the cancellation and the reinforcement in practically the same way, and, therefore, $\langle\mu^2\rangle$ remains almost unchanged.

We conclude by saying that the four-states scheme developed by Yarim-Agaev et al.[5] for oligomers of PMA can also be applied to phenyl and chlorophenyl esters. Among the five conformational parameters used in the calculation, ρ is independent of the kind of ester, while the other four depend strongly on the chemical structure of the alcoholic residue of the ester.

Acknowledgment. Partial support of this work by the CICYT, through Grant PB-86-0620, is gratefully acknowledged.

Registry No. PDG, 117341-06-7; PCPDG, 117341-07-8; OCPDG, 117341-09-0; MCPDG, 117341-08-9.

References and Notes

(1) Riande, E.; Madruga, E. L.; San Román, J.; Saiz, E. *Macromolecules* **1988**, *21*, 2807.
(2) Yoon, D. Y.; Suter, U. W.; Sundararajan, P. R.; Flory, P. J. *Macromolecules* **1975**, *8*, 784.
(3) Ojalvo, E. A.; Saiz, E.; Masegosa R. M.; Hernández-Fuentes, I. *Macromolecules* **1979**, *12*, 865.
(4) Tarazona, M. P.; Saiz, E. *Macromolecules* **1983**, *16*, 1128.
(5) Yarim-Agaev, Y.; Plavsic, M.; Flory, P. J. *Polym. Prepr. (Am. Chem. Soc., Div. Polym. Chem.)* **1983**, *24*(1), 233.
(6) Saiz, E.; Riande, E.; Mark, J. E. *Macromolecules* **1984**, *17*, 899.
(7) Doskocilova, D.; Schneider, B. *J. Polym. Sci., Polym Lett.* **1965**, *3*, 213.
(8) Doskocilova, D.; Stokr, J.; Pivcova, H.; Obereigner, B.; Lim, D. *J. Polym. Sci., Part C* **1968**, *23*, 365.
(9) Bovey, F. A. *Chain Structure and Conformation of Macromolecules*; Academic Press: New York, 1982.
(10) Riande, E. *J. Polym. Sci., Polym. Phys. Ed.* **1976**, *14*, 231.
(11) Guggenheim, E. A. *Trans. Faraday Soc.* **1949**, *45*, 714.
(12) Smith, J. W. *Trans. Faraday Soc.* **1950**, *46*, 394.
(13) MacClelan, A. L. *Tables of Experimental Dipole Moments*; Rahara: El Cerrito, CA, 1974; Vol. 2.
(14) Le Fevre, R. J. W.; Sundaram, A. *J. Chem. Soc.* **1962**, 3904.
(15) Saiz, E.; Hummel, J. P.; Flory, P. J.; Plavsic, M. *J. Phys. Chem.* **1981**, *85*, 3211.
(16) Suter, U. W.; Flory, P. J. *J. Chem. Soc., Faraday Trans. 2* **1977**, *73*, 1521.
(17) Flory, P. J. *Statistical Mechanics of Chain Molecules*; Interscience: New York, 1969.
(18) Hummel, J. P.; Flory, P. J. *Macromolecules* **1980**, *13*, 479.

Infrared Dichroism Measurements of Molecular Relaxation in Binary Blend Melt Rheology

Julia A. Kornfield and Gerald G. Fuller*

Chemical Engineering Department, Stanford University, Stanford, California 94305

Dale S. Pearson

Department of Chemical and Nuclear Engineering and Materials Department, University of California, Santa Barbara, California 93106. *Received May 24, 1988; Revised Manuscript Received August 3, 1988*

ABSTRACT: A new rheooptical technique to measure dynamic infrared dichroism was used with deuterium labeling to observe the relaxation of each molecular weight component in a bidisperse entangled polymer melt. The bulk relaxation is measured simultaneously by using birefringence. The relaxation dynamics of the bulk and of each component depend upon the two polymer relaxation times and the blend ratio. Nearly monodisperse pairs of hydrogenated and deuteriated polyisoprenes of molecular weights 53 000 and 370 000, both several times the entanglement molecular weight, were used. Results for the linear viscoelastic step shear strain relaxation of each component and of the bulk for blends containing 10, 20, 30, 50, and 75 vol % long chains are presented. The component dynamics are qualitatively predicted by current molecular theories of polymer melt rheology; however, some important differences are observed. In particular, it was found that polydispersity can strongly retard the orientational relaxation of the low molecular weight component and decrease the longest relaxation time of the high molecular weight component.

I. Introduction

The rheology of entangled polymer melts has been the subject of a large number of experimental studies and theoretical investigations. Industrial polymer melts typically have a broad distribution of molecular weights which strongly affects their viscoelastic properties. The complexity of these effects in an arbitrary molecular weight distribution has motivated researchers to study model polydisperse systems. Binary blends of well-characterized, nearly monodisperse, linear polymers of different molecular weights have proven to be simple, well-defined systems for investigation. Traditionally the goal of research on binary blends has been to determine appropriate blending

* Author to whom correspondence should be addressed.

0024-9297/89/2222-1334$01.50/0

laws relating rheological properties to the molecular weight distribution.[1-3] In recent years, new molecular theories for the dynamics of polymer melts[4-11] have stimulated experimentalists to reexamine the molecular relaxation processes which occur in polymer melts. While most of the current studies use monodisperse polymers, they include additional studies of the viscoelasticity of binary blends,[12-15] as well as studies of matrix effects on diffusion[16-18] and relaxation dynamics.[19,20]

A clearer appreciation for the complexity of the dynamics of polymers in polydisperse melts has emerged from experiments on bimodal molecular weight systems.[21] Even for this relatively simple case, there is a complex dependence on the three independent parameters: the molecular weight of the long polymer, M_L; the molecular weight of the short polymer, M_S; and the volume fraction of the long polymer, Φ_L. In a melt in which both M_L and M_S are well above the critical molecular weight for entanglement, and have approximately the same molecular weight, reptation is expected to be the dominant molecular motion of both species, as it is in a monodisperse melt of either species. As the difference between the two molecular weights increases, the difference between the two reptation times, τ_S and τ_L, rapidly increases since the reptation times vary approximately as M^3. Therefore the matrix of topological constraints surrounding the long polymer will not appear fixed, and the long chains will have another mode of relaxation due to the dynamics of the matrix.

In diffusion experiments,[17] it has been observed that the motion of sufficiently high molecular weight long chains in a matrix of short chains is independent of matrix molecular weight for matrix chains above a length given by $M_S^3 > 10M_e^2M_L$, where M_e is the molecular weight between entanglements. As the matrix molecular weight M_S is decreased below this threshold, the diffusion coefficient of the long chains, D_L, increases dramatically in two stages. First, for matrix chains below the threshold but still long enough to be entangled, D_L increases as M_S^{-3}; then, as M_S decreases further, so that the matrix chains are no longer entangled, D_L increases as $1/M_S$.

From these infinite dilution diffusion results it is clear that even the binary blend case involves numerous regimes depending upon the molecular weights M_L and M_S. One regime is the range of short-chain molecular weights in which the long-chain diffusion is unaffected by the matrix: $M_L > M_S > 10(M_e/M_S)^2M_L$. For M_L many times M_e, this regime includes a large range of M_S. Therefore one can select M_S such that $M_L \gg M_S \gg 10(M_e/M_S)^2M_L$, which provides a large separation in the reptation times of the two species, while preserving the same diffusional behavior each species would have in a monodisperse matrix.

Studies of the linear viscoelasticity of such binary blends indicate that the long-chain contribution to the relaxation modulus is substantially affected by the amount of short chains in the matrix, even though the long-chain diffusion is not.[15] These effects have been described in terms of an additional mode of relaxation afforded the long chains by the release of short-chain constraints. Reptation-based theories that incorporate the effects of constraint release have been developed.[8-11] Reasonable agreement of constraint release theories with the bulk rheology motivated this research to provide a more quantitative test by measuring the dynamics of each component. Although considerable efforts have been made to extract information about the dynamics of each component from mechanical rheometric measurements, success has been limited only to inferring features of the terminal relaxation of the long polymer.[12,15]

In this paper, a new optical rheometric technique is described and applied to binary blends to measure not only the total relaxation modulus but also the contribution of each molecular weight component. Binary blends of chains of two molecular weights, M_S and M_L, were prepared with different volume fractions of long polymer, Φ_L. Linear viscoelastic step-strain relaxation experiments on these blends provide a direct measurement of the relaxation of the long chains and of the short chains as functions of the blend ratio. On the basis of earlier diffusion studies[17] discussed above, the diffusion of the long chains should not be affected by constraint release for the molecular weights used. Therefore, the results of these experiments can be used to test the predictions of constraint release models for the dynamics of each molecular weight component.

The measured quantities in these experiments are the birefringence and dichroism that occur when a polymer is under stress. Measurements are performed at the infrared wavelength of the carbon–deuterium stretching vibrational absorption. As is explained in the next section, this choice of wavelength makes it possible to optically label a polymer by substitution of hydrogen with deuterium. The dichroism observed is related to the contribution to the stress due to the chains that contain carbon–deuterium bonds. The stress–optical coefficient for birefringence is not affected by the substitution of a small fraction of deuterium for hydrogen, so that the birefringence provides a measure of the bulk stress. Comparison of birefringence and relaxation modulus measurements for these blends is used to verify that the stress–optical rule is applicable.

Infrared dichroism has been applied to the study of polymers for many years. Currently a number of workers use Fourier transform infrared dichroism spectroscopy to study orientational dynamics in polymers.[20,22-25] The present method is a fixed-wavelength polarimetry technique rather than a spectroscopic one. It is distinguished from other infrared dichroism techniques by its high sensitivity, fast time response, and simultaneous measurement of birefringence and dichroism. As a result of its sensitivity, the present method is the first to allow infrared dichroism measurements under shear flow and with small enough strains to study linear viscoelasticity. Section II below is devoted to a discussion of the theoretical basis of this technique and the design of the experimental apparatus.

This study of molecular dynamics in binary blends requires matched pairs of labeled and unlabeled monodisperse linear polymers of the same degree of polymerization. For each blend ratio, two samples are prepared, one with only long chains labeled and the other with only short chains labeled. A perfect labeling technique would not alter the molecular weight distribution, molecular dynamics, or thermodynamic properties of the polymers and would therefore give identical rheological properties regardless of which chains are labeled. To approach this ideal, hydrogenated and deuteriated derivatives of ionically polymerized polyisoprenes are used as unlabeled and labeled polymer pairs. The labeled polymers have a fairly low degree of deuteriation and are used in low concentration, minimizing the potential for isotopically driven phase separation.[26,27] The synthesis, characterization, and thermodynamics of the polymers are discussed in section III.

The methods used in preparing the series of blends, and in performing mechanical and optical step-strain relaxation experiments, are described in section IV. Results of

these measurements are presented in section V. The implications of our observations for molecular models are discussed in the concluding section.

II. Infrared Dichroism and Birefringence

A. Theoretical Basis of Experiment. We have built an apparatus for the simultaneous measurement of birefringence and dichroism at a fixed wavelength in the infrared. In this section, the relationship of these two observables to the rheological response of a binary blend melt is discussed.

The orientational state of each polymer chain can be described in terms of Rouse segments specified by the set of position vectors R_{ni} or by the set of bond vectors r_{ni}, where subscript n denotes the index of the segment and i denotes the vector component. In a melt consisting of two discrete molecular weight components, both composed of identical monomer units, the "short" and "long" chains contain N_S and N_L Rouse segments, respectively. Since they are composed of identical monomer units, all chains have the same mean square segment length, b^2. The orientation distribution of segments in the system is described by the distribution function $\Psi(\{r_{ni}\})$.

At any instant, the state of stress in the melt is related to the second moment of the orientation distribution of chain segments by[28]

$$\sigma_{ij} = (3k_BT/b^2)c\langle r_i r_j\rangle + P\delta_{ij} \tag{1}$$

where σ_{ij} is the stress tensor, k_BT is Boltzmann's constant times absolute temperature, c is the number of segments per unit volume, P is the pressure, and $\langle r_i r_j\rangle$ is the second moment tensor of the orientation distribution of Rouse segments, defined as

$$\langle r_i r_j\rangle = (1/N)\sum_{n=1}^{N}\left[\int \mathrm{d}\{r_{mi}\}_N\, \Psi(\{r_{mi}\}_N) r_{ni} r_{nj}\right] \tag{2}$$

The average is taken over the segments in an arbitrary control volume V containing $N = cV$ segments; the factor of $1/N$ gives $\langle r_i r_j\rangle$ on a per segment basis. Equation 1 for the stress is valid so long as the polymers are not so extended that the Gaussian approximation for the orientation distribution breaks down.

Conceptually, the average over all chain segments can be written as the weighted sum of the average over segments belonging to long chains and the average over segments belonging to short chains. The second moment of the orientation distribution of Rouse segments on a K chain $\langle r_i r_j\rangle_K$ is defined as

$$\langle r_i r_j\rangle_K = (1/N_K)\sum_{n=1}^{N_K}\left[\int \mathrm{d}\{r_{mi}\}_K\, \Psi_K(\{r_{mi}\}_K) r_{ni} r_{nj}\right] \tag{3}$$

where the subscript K is either L for long or S for short chains, the integration is over segments on a K chain, the Ψ_K denotes the orientation distribution function for K chain segments. Here the factor of $1/N_K$ gives $\langle r_i r_j\rangle_K$ on a per segment basis. Since the segment volume is taken to be the same on long and short chains, it follows that the second-moment tensor as defined in eq 2 equals the volume-weighted average of the second-moment tensors of the two components:

$$\langle r_i r_j\rangle = \Phi_L\langle r_i r_j\rangle_L + \Phi_S\langle r_i r_j\rangle_S \tag{4}$$

Thus the stress tensor can be written as

$$\sigma_{ij} = (3k_BT/b^2)c[\Phi_L\langle r_i r_j\rangle_L + \Phi_S\langle r_i r_j\rangle_S] + P\delta_{ij} \tag{5}$$

where Φ_L and Φ_S are the volume fraction of long and short chains, respectively.

Although previous experimental techniques could not observe the stress contributions broken down in this way, the optical technique presented here can. This is possible because the refractive index tensor, like the stress tensor, is fundamentally related to the orientation distribution of segments, but unlike the stress tensor, it is amenable to labeling.

Since birefringence and dichroism are measures of optical anisotropy, we are concerned only with the deviatoric part of the full refractive index tensor

$$n_{ij} = \hat{n}_{ij} - \tfrac{1}{3}n\delta_{ij}$$

where the isotropic refractive index n is subtracted from the total, $\hat{n}_{ij}$. The deviatoric refractive index n_{ij} of the material can be written as a sum of real and imaginary parts:

$$n_{ij} = n_{ij}' + in_{ij}''$$

The real part describes how the material retards light, and the imaginary part describes how it attenuates light.

Anisotropy in the refractive index of a polymeric liquid is fundamentally related to anisotropy in the orientation distribution of polymer segments. Gaussian chain statistics and additivity of the polarizability lead to a relationship between the deviatoric polarizability tensor and the orientation of segments which must be of the form[29]

$$\alpha_{ij} - \tfrac{1}{3}\alpha\delta_{ij} = A\langle r_i r_j - \tfrac{1}{3}r^2\delta_{ij}\rangle \tag{6}$$

where α_{ij} is the full polarizability tensor, α is the isotropic component of the polarizability, and A is a constant. The polarizability is related to the real part of the refractive index of the material through the Claussius–Mosotti equation. For the usual case of small anisotropy, this relationship may be linearized to derive the following relationship between the deviatoric parts of the real part of the refractive index tensor and the second-moment tensor:[30]

$$n_{ij}' = 2\frac{\pi}{9}\frac{(n^2+2)^2}{n}A\left\langle r_i r_j - \frac{1}{3}r^2\delta_{ij}\right\rangle \tag{7}$$

By inspection of eq 1, the real part of the deviatoric refractive index tensor is proportional to the deviatoric stress tensor. It is this relationship which underlies the familiar stress–optical rule.

The imaginary part of the refractive index tensor, n_{ij}'', describes the anisotropy in attenuation of light as it passes through the sample. At infrared wavelengths, this component of the refractive index has a strong wavelength dependence determined by the absorption spectrum of the polymer. Suppose that one of the components in the binary blend may be tagged in such a way that one of its absorption peaks is shifted to a wavelength at which it would otherwise be transparent. K, either L for long or S for short chains, designates the tagged component. Vibrational absorption of a photon is polarization dependent and so is associated with a transition moment vector which is directly related to the bond orientations. For the case of an optically thin sample, n_{ij}'' is proportional to the deviatoric part of the second-moment tensor of these transition moment vectors.[31] At a wavelength at which the K chains absorb, but the other chains do not, and with the assumption that the statistics of the K chains are Gaussian, appropriate for an entangled melt, the following expression[29] is obtained:

$$n_{ij}'' = C(\lambda)\langle r_i r_j - \tfrac{1}{3}r^2\delta_{ij}\rangle_K \tag{8}$$

where C is a constant which depends on wavelength λ.

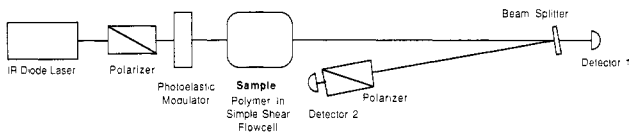

Figure 1. Schematic diagram of the optical train used in the apparatus for simultaneous measurement of infrared dichroism and birefringence. Refer to the text for a detailed description.

Therefore the imaginary part of the deviatoric refractive index tensor, eq 8, is proportional to the contribution of the K chains, either long or short, to the deviatoric stress tensor, eq 5.

An important modification of this view results if a nematic-like interaction,[32-36] i.e., short-range orientational coupling between polymers in the melt, is taken into account.[37-39] The optical anisotropy of a polymer under stress arises at the level of the orientation distribution of chemical bonds along the chain; however, the stress arises from the entropic elasticity associated with statistical segments (Rouse segments or "bonds") composed of many chemical bonds. While it has been shown that the orientation distribution of bonds and of Rouse segments is proportional for the bulk, this may not be the case component by component. In eq 8 it is assumed that the orientation distribution of the bonds which give rise to the dichroism n_{ij}'' is the same as that of the Rouse segments along a K chain. Doi et al.[39] point out that nematic interaction enhances the orientational order at the level of bonds relative to the order on the level of Rouse segments. This alters eq 7 for the birefringence only in the value of the constant A. Applied to each component, however, the result of nematic orientation is a contribution to the orientation of bonds along K chains, which reflects the orientational order of the mean field surrounding a K chain. This leads to the following expression for the dichroism of a sample with K chains labeled (see the Appendix for details):

$$n_{ij}'' = C(\lambda)[\langle r_i r_j - \tfrac{1}{3}r^2\delta_{ij}\rangle_K + (\epsilon/(1-\epsilon))\langle r_i r_j - \tfrac{1}{3}r^2\delta_{ij}\rangle] \quad (9)$$

Comparison of eq 8 and 9 shows the addition of a bulk Rouse segment orientation distribution term to the K chain dichroism.

Equations 7 and 9 give the relationship between the refractive index tensor, n_{ij}, and the orientation of Rouse segments, $\langle r_i r_j\rangle$. When light is passed through the polymeric liquid, the projection of n_{ij} in the plane perpendicular to the beam describes how the light is altered during propagation through the sample. Experimentally it is possible to measure the difference of the two eigenvalues of the chosen projection of n_{ij}: the imaginary part of this difference is the dichroism, and the real part is the birefringence. For this idealized polymer system and the associated choice of wavelength for observation, the dichroism provides a measure of the bond orientational order in the labeled chains. When the nematic coupling contribution to the bond orientation is small, the dichroism gives a measure of the K chain contribution to the stress.

B. Optical Train. In this section the light source, optical train, flow cell, and detectors are described. A schematic diagram of our apparatus is shown in Figure 1. This experimental arrangement is a modification of an earlier optical train developed in our laboratory to measure simultaneously linear birefringence and dichroism at visible wavelengths.[40]

The light source for this experiment is a relatively powerful diode laser with a frequency range of 2180–2195 cm^{-1} and a continuous power rating of greater than 10 mW

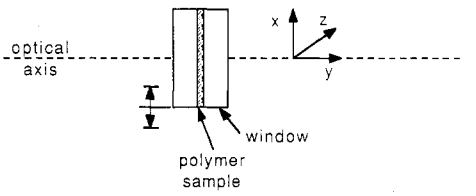

Figure 2. Flow cell geometry showing the optical axis parallel to the y-axis and normal to the parallel plates of the shear flow cell, shown as open rectangles. Shear is applied to the sample between the plates by translating one of the rock salt plates in the x-direction as indicated.

(Spectra Physics SP5800 Laser Source Assembly). The collimated beam passes through incident optics before impinging on the sample. The first two optical elements are a Brewster angle polarizer (Cleveland Crystals Model 1600 IR Polarizer) oriented at 0° and a zinc selenide photoelastic modulator (Hinds International Model PEM80 Series II ZS) oriented at 45°, which produces a sinusoidal retardance, δ, of

$$\delta = A_{PEM} \sin(\omega t)$$

at a frequency ω = 84 kHz and adjustable amplitude A_{PEM}.

Next the beam passes through the sample contained in a parallel plate flow cell, which will be described in detail in section II.C. The beam then strikes a beam splitter (sodium chloride window) at a very shallow angle, less than 5° with respect to the optical axis, so the polarization of neither beam is significantly affected. The transmitted beam is observed directly by detector 1. The reflected beam is observed by detector 2 through a second Brewster polarizer oriented at −45°. Both detectors are liquid nitrogen cooled, photovoltaic, indium–antimonide infrared detectors (Santa Barbara Research Center, 2-mm-diameter InSb IR detectors).

The sample is placed in a parallel plate flow cell with the geometry shown in Figure 2. The flow direction, along the x axis, is oriented at 0°. Light passes through the gap, parallel to the y axis. Due to this choice of flow cell geometry, this experiment observes the xz projection of the refractive index tensor:

$$(n_{ij}')_{xz} = B\left\{\begin{bmatrix}\langle xx\rangle & \langle xz\rangle\\ \langle xz\rangle & \langle zz\rangle\end{bmatrix} - \frac{1}{3}r^2\cdot\begin{bmatrix}1 & 0\\ 0 & 1\end{bmatrix}\right\} \quad (10)$$

$$(n_{ij}'')_{xz} = C\left\{\begin{bmatrix}\langle xx\rangle_K & \langle xz\rangle_K\\ \langle xz\rangle_K & \langle zz\rangle_K\end{bmatrix} + \frac{\epsilon}{1-\epsilon}\begin{bmatrix}\langle xx\rangle & \langle xz\rangle\\ \langle xz\rangle & \langle zz\rangle\end{bmatrix} - \frac{1}{1-\epsilon}\cdot\frac{r^2}{3}\begin{bmatrix}1 & 0\\ 0 & 1\end{bmatrix}\right\} \quad (11)$$

where B is $2(\pi/9)((n^2+2)^2/n)A$ from eq 7 and C is from eq 9. Due to the symmetry of this projection about the x axis, $\langle xz\rangle = 0$ and $(n_{ij})_{xz}$ is diagonal. Thus the birefringence and dichroism, the real and imaginary parts of the difference of eigenvalues of $(n_{ij})_{xz}$, are simply the difference of the diagonal elements. It follows that in this projection the birefringence and dichroism are coaxial and oriented parallel to the x axis.

The real part of eq 10 gives a birefringence proportional to $\langle xx\rangle - \langle zz\rangle$; by eq 1 this is proportional to $\sigma_{xx} - \sigma_{zz}$, the third normal stress difference, equal to the sum of the first and second normal stress differences. In relaxation following a step strain, the first normal stress difference is proportional to the shear stress.[41] Furthermore, for materials which show time–strain separable behavior, the time dependence of the first and second normal stress differences is the same. The Doi–Edwards theory, for example,

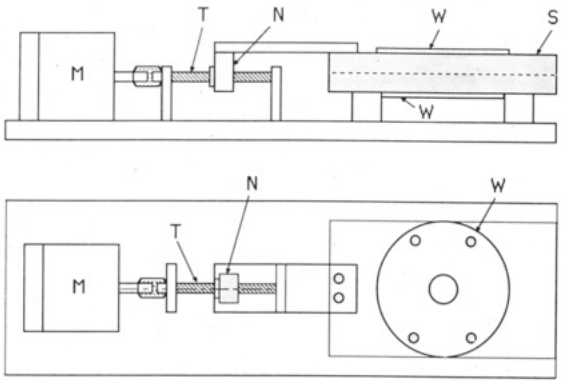

Figure 3. Flow cell design for device to produce abrupt shear strain. M, stepping motor; T, threaded shaft; N, nut to drive translation; W, window holder; and S, translation stage. Refer to the text for a detailed description.

predicts time–strain separable behavior for polymer melts.[5] This prediction has been borne out in experimental studies of melts and solutions.[42] However, there are constitutive models (e.g., Leonov)[43] which predict different time dependences for the first and second normal stress differences. Here we will take as an additional assumption that the sum of the first and second normal stress differences is proportional to the shear stress. Then, following a step strain, the birefringence relaxation is proportional to the shear stress relaxation modulus.

The imaginary part of $(n_{ij})_{xz}$ arises only from the tagged K chains. From eq 9, this will be due in part to the contribution of the K chains to the third normal stress difference and in part to the nematic coupling to the total third normal stress difference. It follows from the additivity of the components' contributions to the stress tensor, eq 5, that when the preceding assumption of proportionality between the normal stresses and the shear stress holds for the bulk it will hold for the Rouse segment orientation distribution of each component as well. When the dominant term in eq 9 is that due to the orientation of the K chain on the level of Rouse segments, the dichroism provides a direct measure of the contribution of the K chains to the stress. When the contribution of the Rouse segment orientation and of the nematic orientation are of the same order, the dichroism does not have this simple interpretation.

C. Flow Cell Design. The flow cell is shown schematically in Figure 3. The upper diagram shows a view of the side of the flow cell; the lower diagram shows a front view. The plates in this flow cell are sodium chloride windows, held in a translator. Parallel motion is provided by a translation stage (NRC Model 435A-0MA) which uses precision cross cylindrical bearings. This model has vertical and lateral deviation of position of less than ±0.0001 in./in. of travel.

To mount the windows to the stage, aluminum holders were machined to tolerances of ±0.0005 in. The clear aperture of the device is through a slot cut in the front holder and a 0.25-in.-diameter hole in the back holder. Precision spacer gaskets machined from shim stocks of thickness from 0.002 to 0.125 in. were used to adjust the gap width between the windows. These were placed between the holder and stage, allowing fine adjustment of the gap while maintaining a secure, parallel attachment of the windows to the translation stage.

To load the flow cell, the polymer is placed on the center of the back window. Then the back holder is inserted in the opening in the back of the translation stage and bolted down. The gap width for the sample is fixed by spacers selected and placed on the shoulder of the front window holder. The front holder is then inserted into the translation stage, pressing the front window against the sample. As the front holder is slowly bolted in, the sample is squeezed down to the desired gap thickness.

Step strains are applied to the sample by abrupt translation of one window. A precision stepping motor (25 000 steps/revolution, Compumotor) turns a threaded shaft (80 threads/in.) to drive the translation. Control of the amplitude and timing of the displacement are achieved by interfacing the motor controller to a microcomputer. The strain applied to the sample is measured by using a voltage–displacement transducer mounted on the flow cell.

D. Signal Processing and Data Collection. The optical train is readily analyzed by using the Mueller formalism.[44] This analysis gives the relationship between the experimental variables and the amplitude of harmonics of the PEM carrier frequency ω in the intensity observed by each detector. The intensity signal measured by either detector is of the form

$$I^{(i)} = I^{(i)}_{DC} + I^{(i)}_{\omega} \sin(\omega t) + I^{(i)}_{2\omega} \cos(2\omega t) + \ldots$$

For detector 1, the amplitude of the second harmonic, $I^{(1)}_{2\omega}$, is

$$I^{(1)}_{2\omega} = I^{(1)}_0 J^{(1)}_2 A_{PEM} \sinh \nu$$

where $I^{(1)}_0$ is the beam intensity after the first polarizer multiplied by the fraction transmitted by the beam splitter, $J^{(1)}_2(A_{PEM})$ is the value of the Bessel function, and ν is proportional to the dichroism:

$$\nu = (2\pi d/\lambda)\Delta n''$$

λ is the wavelength of light, d is the sample path length, and $\Delta n''$ is the dichroism, equal to the difference in the eigenvalues of the imaginary part of the observed projection of the refractive index tensor. For detector 2, the first harmonic, $I^{(2)}_{\omega}$, is

$$I^{(2)}_{\omega} = I^{(2)}_0 J^{(2)}_1 A_{PEM} \sin \mu$$

where $I^{(2)}_0$ is the beam intensity after the first polarizer multiplied by the fraction reflected by the beam splitter, $J^{(2)}_1(A_{PEM})$ is the value of the Bessel function, and μ is proportional to the birefringence:

$$\mu = (2\pi d/\lambda)\Delta n'$$

$\Delta n'$ is the birefringence, defined as the difference in the eigenvalues of the real part of the observed projection of the refractive index tensor.

In our experiments μ is of order 10^{-1} and ν is of order 10^{-3}. Therefore, sinh ν and sin μ approximately equal their arguments, ν and μ. In this case, the second harmonic of the signal from detector 1, $I^{(1)}_{2\omega}$, is proportional to the dichroism, and the first harmonic of the signal from detector 2, $I^{(2)}_{\omega}$, is proportional to the birefringence.

The electronics for demodulating the signals from the detectors and collecting the data are similar to those described by Johnson et al.[40] The reference signal from the PEM is provided to two lock-in amplifiers. Output from detector 1 is sent through a high-speed preamp and then to one of the lock-ins, set for a reference frequency of 2ω. The signal from detector 2 is similarly amplified and sent to the other lock-in, set to a reference frequency of ω. The outputs of the two lock-in amplifiers and of the displacement transducer on the flow cell are simultaneously recorded by using a digital storage oscilloscope. Each trace is then transferred to a microcomputer. Fifteen to forty-five step strain experiments were recorded and averaged for each blend ratio studied.

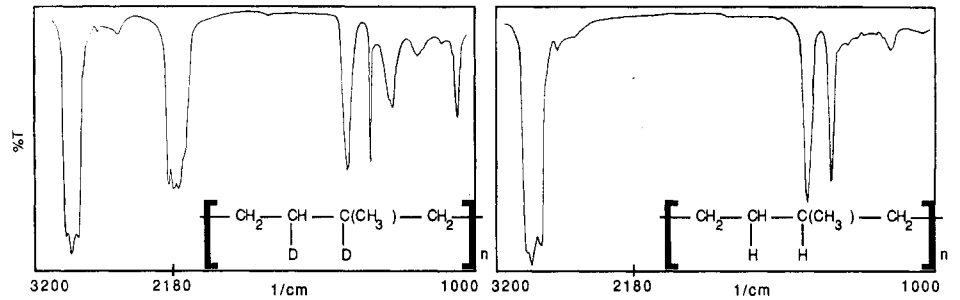

Figure 4. Infrared spectra of the labeled (deuteriated polyisoprene, DPI), normal (hydrogenated polyisoprene, HPI), and ideal monomer structures.

III. Polymer Synthesis and Characterization

A. Synthesis of Hydrogenated and Deuteriated Polyisoprene. The polyisoprenes used in this study were synthesized by L. J. Fetters. The method consisted of anionically polymerizing isoprene with *sec*-butyllithium in a solvent consisting of a 95/5 cyclohexane/benzene mixture. The reaction took place at room temperature. After 1 day the living anions were terminated with dry, degassed methanol, and the polymer was isolated by precipitation in 2-propanol. After drying, the material was redissolved in cyclohexane and then charged to a reactor in which it was saturated with either hydrogen or deuterium, with palladium on calcium carbonate as the catalyst. Further details on the polymerization and saturation procedures can be found in the literature.[45,46]

B. Microstructure and Molecular Weight Distribution. The microstructure of the polyisoprene materials was approximately 70% cis, 23% trans, and 7% 3,4 units as determined by proton NMR. The NMR spectra of the same polymers after reaction with hydrogen or deuterium showed that the level of unsaturation was reduced to less than 0.3%. It was further revealed by deuterium NMR using deuteriochloroform as an internal standard that saturation with deuterium was accompanied by deuterium exchange for some of the protons. If saturation but no exchange took place, each isoprene monomer would contain two deuterium atoms and the weight fraction of deuterium would be 0.056. The two deuteriated polymers used in this study, S-DPI and L-DPI, contain 0.104 and 0.098 weight fraction deuterium, respectively.

The molecular weights of the polymers were determined by more than one method. The polyisoprene polymers were analyzed by gel permeation chromatography (GPC) using a refractive index detector, by measuring the intrinsic viscosity, and by low-angle laser light scattering. A chromatograph equipped with refractive index and light-scattering detectors was used for the saturated polymers. Both chromatographs were calibrated with appropriate polymer standards (polyisoprene and polyethylene). The molecular weights obtained in this way are reported in Table I. Using the values given there, the weight-average molecular weights of the short and long polymers are estimated to be 53 000 and 370 000, which correspond to degrees of polymerization of 780 and 5440.

The infrared spectra of S-HPI and S-DPI are shown in Figure 4, along with the ideal monomer unit for the normal and labeled polymer. Here we do not undertake a detailed analysis of the infrared spectra but point out the general contrast between the normal and labeled polymer spectra. Comparison of the spectrum of S-DPI with that of S-HPI shows the appearance of a number of new absorption peaks which involve carbon–deuterium bonds. Among these new peaks, the carbon–deuterium stretching peak is relatively strong and occurs at 2180 cm^{-1}, in a frequency range where the normal polymer does not absorb significantly. At this frequency, then, the assumption that only the labeled polymer contributes to attenuation, and hence to the dichroism, is a good one.

Table I
Molecular Weight Determination

	polyisoprene[a]		hydrogenated polyisoprene	
sample	mol wt	M_w/M_n	mol wt	M_w/M_n
S-HPI	54 000[b]	1.04[b]	48 000[e]	1.05[e]
	52 000[c]		52 000[f]	
L-HPI	366 000[b]	1.05[b]	323 000[e]	1.47[e]
	366 000[c]		302 000[f]	
	357 000[d]			

[a] Polyisoprene molecular weight should be increased by a factor of 1.03 to account for change on hydrogenation. [b] GPC in tetrahydrofuran at 25 °C. [c] From intrinsic viscosity in cyclohexane at 25 °C. [d] Light scattering in cyclohexane at 25 °C. [e] GPC in trichlorobenzene at 135 °C. [f] Light scattering in trichlorobenzene at 135 °C.

C. Thermodynamic Considerations. One of the fundamental assumptions behind these experiments is that the deuterium labeling has no effect on chain dynamics. This seems a reasonable approximation on the basis that the substitution of a small fraction of the hydrogen atoms with deuterium is expected to have only a very slight effect on the local chain dynamics. However, it has been shown by Bates et al. that deuterium labeling can produce isotopically driven phase separation in binary mixtures of perdeuteriated and normal polymers.[26] These observations indicate that the analysis of Buckingham and Hentschel accurately describes this phenomena.[27] The driving force for incompatibility is the small decrease in monomer volume that results from deuterium substitution. The potential for phase separation increases with molecular weight and decreases with increasing temperature. In this study lightly deuteriated polymer was used as the labeled species. All of our experiments were performed at 25 °C with a 0.1 volume fraction of labeled polymer. The blend with the greatest molecular weight, hence the most likely to phase separate, is one of 10% labeled long polymer, with 90% unlabeled long polymer.

In the case of two polymers of the same molecular weight, the upper critical point occurs for a blend of equal parts of the hydrogenated and deuteriated species. Thus, to conservatively evaluate the potential for phase separation in our experiments, we consider a 50:50 blend of unlabeled and normal long chains. For this case we determined that a change in monomeric volume due to deuteriation, $\Delta V/V > 3.3 \times 10^{-3}$, would be necessary to cause phase separation at 25 °C in a blend of equal parts of HPI and DPI of the degree of polymerization of our long chains, $N_L = 5440$. This is comparable to the value of $\Delta V/V$ observed for perdeuteriated polybutadiene. Although we did not measure the value $\Delta V/V$ produced by the light deuteriation employed in this study, it should certainly be

well below that produced by perdeuteriating a polymer of similar monomer size. We concluded that phase separation at 25 °C can be ruled out for any of the blends used in these experiments.

IV. Methods

A. Preparation of Blends. The melts used in this study were prepared by blending "short" saturated polyisoprene chains, S-HPI and S-DPI, of degree of polymerization N_S = 780, with "long" saturated polyisoprene chains, L-HPI and L-DPI, with N_L = 5440. For each blend ratio of long to short chains, three samples were prepared. The mechanical experiments were performed on blends of hydrogenated polymers, S-HPI and L-HPI. The optical experiments were performed on two samples for each blend ratio, one containing some deuteriated short chains and the other containing some deuteriated long chains. The pairs of labeled samples were prepared by weighing out each component with sufficient precision to determine the blend ratio with an accuracy of 0.2%, and the deviation in volume fraction of long chains for blends of the same nominal blend ratio was kept below 0.005.

To blend the polymers, the samples were dissolved in excess cyclohexane (Aldrich Gold Label) with gentle agitation at room temperature for 24–48 h. The polymer was then cast from the solution onto an aluminum plate where most of the solvent was allowed to evaporate. To continue drying, the blends were stored at room temperature in a vacuum desiccator. Samples were typically allowed to dry under vacuum for at least a few weeks before they were used in experiments. For most samples experiments were repeated many weeks apart to check for artifacts due to incomplete removal of cyclohexane.

B. Mechanical Rheological Measurements. Rheological measurements were performed with a Rheometrics System Four rheometer equipped with parallel disk test fixtures. Step strains of 10% or less were applied by rapidly rotating the upper disk to the desired position with a rise time of ~30 ms. Voltages from the torque transducer were then acquired by a microcomputer until the signal decayed to zero. All experiments were performed at small enough strains so that the stress relaxation modulus, $G(t)$, was independent of the applied strain. Additional experiments were performed to measure the dynamic moduli of linear viscoelasticity, $G'(\omega)$ and $G''(\omega)$, the results of which will be reported in a separate publication.[47] In either case, the rheological response of the pure protonated and the pure deuteriated polymers could be superimposed on each other with no discernible differences.

C. Optical Rheological Measurements. All of the optical experiments were conducted at room temperature. Sample thicknesses of 0.015–0.025 in. were used, and step strains of 15–30% were applied. The rise time for step strains was under 100 ms for all samples. A typical strain history is shown in Figure 5a. This linear voltage displacement transducer (LVDT) output was recorded for a step strain applied to a sample with a 0.75 volume fraction of long chains, with short chains labeled. The strain shows a rise time of 90 ms to 97% of the ultimate strain. At 150 ms the displacement passes through its desired value, after which there is a slight overshoot of 1% of the total strain, which was recovered over the first few seconds. The ultimate total displacement was 0.0044 in. The gap for this experiment was 0.015 ± 0.001 in., so the step strain was 29% ± 2%. This is still within the range of linear viscoelasticity since entangled polymeric liquids show only slight deviation from linear behavior to rapid shear strains as large as 50% or more.[48,49]

Raw data for the birefringence for this particular experiment are shown in Figure 5b, while raw dichroism data are shown below in Figure 5c. The dichroism data clearly have a lower signal to noise ratio than the birefringence. This reflects the fact that the birefringence is at least 2 orders of magnitude larger than the dichroism. The optimal signal to noise ratio for the dichroism is determined by the trade off between transmitted light intensity and concentration of labeled polymer. Increasing the concentration of labeled chains increases the dichroism of the sample for a given gap width and strain, but it decreases the transmitted light intensity from which the dichroism is measured. The data reported here are for blends containing 10 vol % labeled polymer. Experiments were repeated and averaged until the signal to noise ratio of the averaged dichroism data was at least 10, referenced to the peak signal.

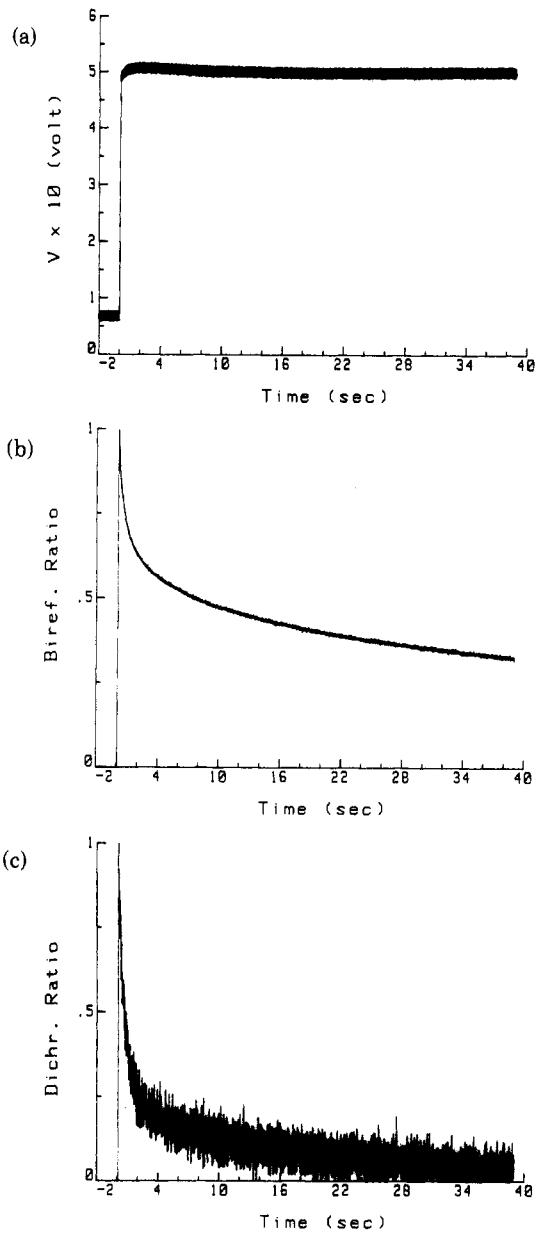

Figure 5. Typical raw data collected for the first 40 s of a step strain relaxation experiment. These results are for a blend which contains 75 vol % long polymer and which contains labeled short chains. (a) Signal from the linear voltage displacement transducer on the flow cell. (b) $I_{\omega}^{(2)}$ from the lock-in amplifier, which demodulates the signal from detector 2. This plot shows the data normalized by the maximum value. The zero value is determined by the long-time base line, at 40 s, for this short-chain birefringence data. (c) $I_{2\omega}^{(1)}$ from the lock-in amplifier, which demodulates the signal from detector 1. The data are shown normalized by the maximum value, and the zero value is determined by the base line at 1500 s for this dichroism data.

These data were reduced by using the long-time base line as zero and the value at approximately 100 ms as unity. This approach is subject to some uncertainty in both the reference zero and unity. For most samples the relaxation of both the birefringence and dichroism was recorded considerably past the time required for the signals to decay to the limit of resolution by our apparatus, and the uncertainty in the reference zero is correspondingly small compared to the signal resolution. The few cases in which there might be greater uncertainty are discussed in the Short-Chain Relaxation section below. Imperfection in synchronization of the experiment leads to uncertainty in the normalization used in our data reduction. The rise time of the optical parallel plate device was found to be sample dependent, and the synchronization to determine time zero was not perfect. The digitized time point closest to 100 ms after the initial rise was

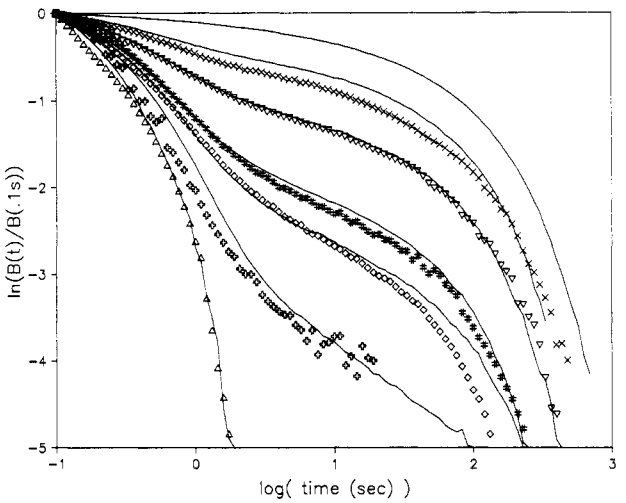

Figure 6. Bulk relaxation following a step strain as measured by stress and birefringence. The solid curves show the normalized relaxation modulus for blends containing 0%, 10%, 20%, 30%, 50%, 75%, and 100% by volume long polymer. The symbols show the normalized birefringence relaxation for blends containing 0% (△), 10% (+), 20% (◇), 30% (#), 50% (▽), and 75% (×) by volume long polymer. Notice that the two independent measurements show close agreement.

used as the first point. The uncertainty in this determination of t = 100 ms is ± 10 ms. The normalized relaxation data were tabulated at logarithmically spaced time points, 25 points/decade out to the end of the trace. These reduced data are shown in Figures 6–8.

V. Results

As the infrared dichroism technique is a new one, the various possible tests of self consistency of the results are important. Therefore this section is devoted not only to presenting the experimental results but also to discussing how these are scrutinized within the theoretical framework for this new technique.

A. Mechanical Relaxation Modulus. An independent rheological characterization of these polymers was performed by measuring the stress relaxation modulus and the dynamic moduli. Normal (HPI) and labeled (DPI) polymers were studied in the monodisperse form, and their rheological properties were found to be indistinguishable. This indicates that the deuteriation does not lead to any observable difference in the rheological properties of monodisperse DPI and HPI of the same degree of polymerization, N. The short polymers, with N_S = 780, were observed to have a relaxation time of 0.35 s. The relaxation time of the long polymers, with N_L = 5440, was 210 s.

A series of binary blends of various volume fractions of long polymer, Φ_L, were prepared from the normal polymers (HPI). The results of the mechanical rheometric characterization of these blends are shown as the solid curves in Figure 6. These results in themselves add to a body of experimental observations of the rheological behavior of bimodal molecular weight distribution linear polymer melts.[15] Within the context of this work, the mechanical results provide a means to test the reliability of the results obtained with our optical flow cell and labeled blends. In addition, mechanical rheometry was used to confirm that the conditions used in our optical experiments are within the range of linear viscoelastic response of this polymer.

B. Birefringence Relaxation Modulus. Optical experiments were performed on samples containing a volume fraction of 10% of labeled polymer. To confirm that the dichroism reflects the orientational anisotropy of the labeled chains, optical experiments were performed on a monodisperse sample of short chains containing 90% HPI and 10% DPI. The birefringence and dichroism were simultaneously recorded for the relaxation of this ample following a step strain. The two sets of data were then

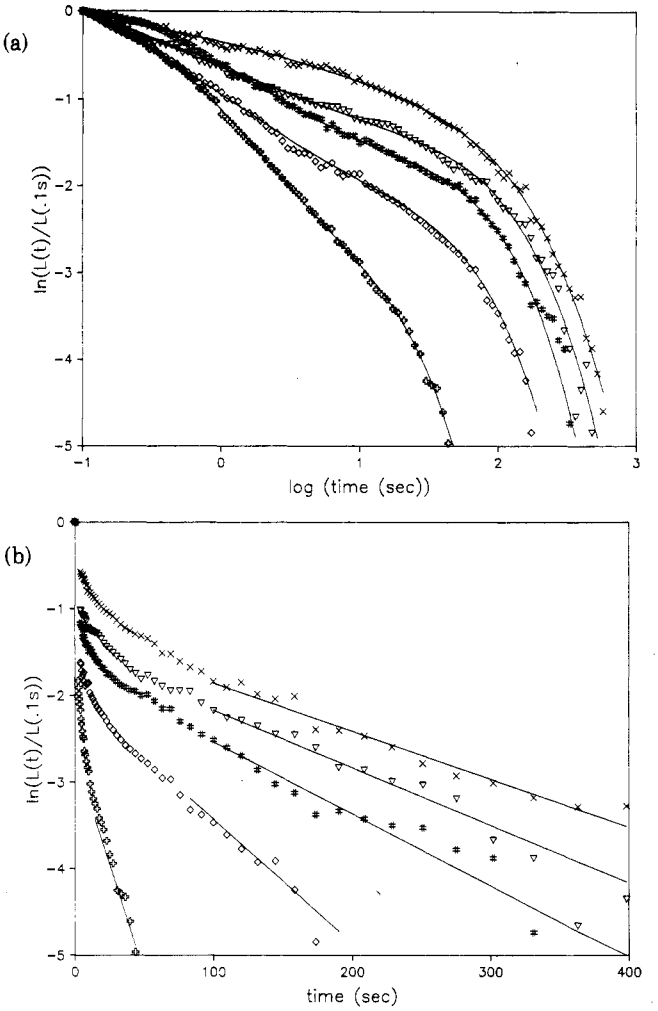

Figure 7. Long-chain dichroism relaxation for blends containing 0% (△), 10% (+), 20% (◇), 30% (#), 50% (▽), and 75% (×) by volume long polymer. (a) log–log plot for comparison with Figure 6. The solid curves are arbitrary smooth curves through the data. (b) Semilog plot to illustrate the effect of molecular weight distribution on the apparent longest relaxation time of the long chains. The solid lines were used to obtain the values of $\tau_{L,app}$ given in Table II.

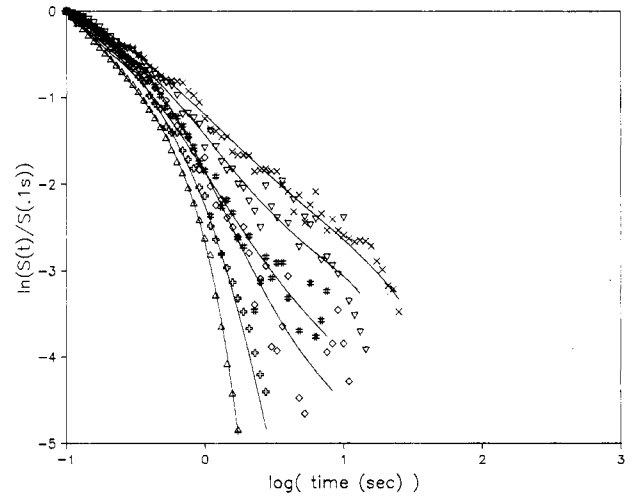

Figure 8. Short-chain dichroism relaxation for blends containing 0% (△), 10% (+), 20% (◇), 30% (#), 50% (▽), and 75% (×) by volume long polymer. The solid curves are arbitrary smooth curves through the data.

normalized and compared. The relaxations of the normalized birefringence and dichroism were found to be indistinguishable in this monodisperse sample. Thus the dynamics of the labeled chains as measured by the dichroism are identical with those of the whole population of chains as measured by the birefringence. This indicates that the labeled and unlabeled chains have identical dynamics in the blend and that the dichroism indeed measures the same segment orientation distribution as the birefringence in this monodisperse system. Thus the results on a monodisperse sample support the assumptions made in deriving eq 8. In the monodisperse case, one cannot distinguish between eq 8 and 9.

Optical experiments were performed on a pair of blends at each volume fraction, one with labeled short chains and the other with labeled long chains. The birefringence relaxations observed for the two blends were compared to check for any discrepancies which might arise from errors in reproducing the desired volume fraction. The agreement was very good in every case. The birefringence relaxation results are shown by the point markers in Figure 6. Each birefringence relaxation function in Figure 6 represents the data on only one blend, selected simply on the basis of signal to noise ratio.

In section II.B it was mentioned that, assuming that the material shows time–strain separable behavior, the birefringence relaxation is expected to be proportional to the relaxation modulus. One can use this comparison to demonstrate the reliability of the experiment. Therefore, the normalized birefringence data were compared with the normalized modulus data to check, for example, that the flow cell adequately produced step strains. By inspection of Figure 6 one can see evidence that the stress and birefringence relaxations are proportional. More quantitatively, the magnitude of the deviation between the normalized relaxation modulus and birefringence was below 0.1 for all times and for all blends but the 10 vol % long blend, in which the deviation was as large as 0.15 near 1 s into the relaxation.

C. Long-Chain Relaxation. For each blend ratio, one blend was prepared with 10 vol % labeled long chains (DPI), the rest of the long chains, and all of the short chains unlabeled (HPI). The dichroism relaxation for these samples provides a measure of the relaxation of the long chains in each blend. The normalized long-chain relaxation results are shown in Figure 7. The data are presented in two ways. For comparison with the modulus and birefringence data, Figure 7a shows a log–log plot on the same scale as Figure 6. To examine the behavior of the longest observable relaxation time, Figure 7b is a semilog plot of the same data.

By comparing Figures 7a and 6, the long-chain relaxation is seen to be slower than that of the bulk. After the short chains in the blend have relaxed, the relaxation of the long chains governs the long-time relaxation of the bulk; therefore, after the short-chain contribution is largely relaxed, the birefringence relaxation and the long-chain relaxation are seen to be proportional. A test of self-consistency of the component relaxation results, which requires the short-chain relaxation data described below, is to examine the appropriately weighted sum of the individual relaxation functions for the long and short polymers as compared to the bulk relaxation. This test was applied to the data for each blend, and the agreement was found to be very good.

The data show that the long-chain relaxation is significantly affected by the addition of short chains to the surrounding matrix, as had been inferred from earlier studies.[12,15] With the addition of short chains to the melt, a fast relaxation of the long chains appears, leading to a decrease in the magnitude of the long-time relaxation shown in Figure 7. For blends of 50% or greater volume fraction of long chains, the longest relaxation time of the long chains is approximately that of monodisperse long chains, and the magnitude of the long-time relaxation falls almost linearly with Φ_L. This observation agrees with the results of previous work on similar binary blends, which show no change in τ_L of blends with $\Phi_L > 0.5$.[15]

Table II
Apparent Longest Relaxation Time

blend Φ_L	$\tau_{L,app}$, s
0.10	20
0.20	70
0.30	120
0.50	150
0.75	180
1.00	200

For smaller volume fractions of long chains ($\Phi_L < 0.5$), however, the longest relaxation time appears to decrease monotonically as Φ_L decreases, as is evident in the semilog plot shown in Figure 7b. The apparent longest relaxation time, $\tau_{L,app}$, calculated from the asymptotes shown in Figure 7b, is given in Table II. These values are consistent with the longest relaxation time determined from both the birefringence and modulus relaxation data. This is expected since the longest relaxation of the bulk is determined by the slowest relaxing species, i.e., the long chains. The apparent reduction in the longest relaxation time has significant implications for molecular theories of melt rheology that will be addressed in the Discussion section.

D. Short-Chain Relaxation. To observe the short-chain relaxation for each blend ratio, a blend was prepared with 10 vol % labeled short chains (DPI), the complement of the short chains, and all of the long chains unlabeled (HPI). The normalized dichroism relaxations for these blends are shown in Figure 8. By inspection of Figures 6 and 8, the short-chain relaxation is visibly faster than that of the bulk for all blends. In addition, the appropriately weighted sum of the short- and long-chain relaxations for each blend was found to agree with the bulk relaxation data, as described above.

The surprising feature about these data is the magnitude of the effect of increasing Φ_L on the short-chain relaxation. In these linear viscoelastic experiments, the diffusive motion of the short chains should be essentially the same in every blend. Therefore, the time required for a short chain to completely diffuse from the initial "tube" of constraints imposed by the mean field just after the strain is applied should remain the same for all Φ_L. As the reptation model applies fairly well for monodisperse melts,[28] this escape time is on the order of the relaxation time of monodisperse short chains, about 0.35 s. However, for the case of 75 vol % long chains, measurable relaxation of the short chains takes place out to tens of seconds. For Φ_L = 0.5 and 0.75, the end of data acquisition (t = 40 s) may have been too early to record the ultimate base line. An error in the base line has little effect on the shape of the curves at short times but causes the terminal relaxation to appear more abrupt than it actually is. Therefore the results in Figure 8 at low signal level, below $\ln(S(t)/S(0.1\text{ s})) = -3$, should be regarded as a lower limit of the true relaxation. The implications of the surprising retardation of the short-chain relaxation for molecular theories are discussed below.

VI. Discussion

The effects of polydispersity in molecular weight on the

rheological properties of entangled polymer melts have proved difficult to model on a molecular level. In a melt composed of short and long chains of fixed molecular weights, the molecular weight distribution can be characterized by the volume fraction of long chains, Φ_L. The relaxation modulus for such a system can be parametrized in terms of the molecular weights of the two components, M_S and M_L, and the molecular weight distribution, Φ_L:

$$G(t) = G(t;M_S,M_L,\Phi_L)$$

The bulk response arises from the response of chains of each molecular weight, and their relaxation may be described by decaying functions $G_S(t;M_S,M_L,\Phi_L)$ and $G_L(t;M_S,M_L,\Phi_L)$. The results presented here show the effects of varying Φ_L, while holding M_S and M_L constant, on G, G_S, and G_L. These measurements were made possible by using optical labeling techniques and polarization modulation optical rheometry.

The experimentally observed component relaxations can be compared with the predictions of molecular models of linear chain melt rheology. Some of the qualitative features are captured by various models which incorporate the effects of constraint release into a reptation-based model.[8-11] In particular, these theories predict that the presence of short chains in the matrix permits a Rouse-like relaxation of the primitive path of the long chains with a hopping time approximately equal to the reptation time of the short chains. This is clearly evident in the relaxation observed for long chains as the volume fraction of short chains increases.

There are a few important features of the component relaxations which are not anticipated by current molecular theories. For long-chain volume fractions less than 0.5, the terminal long-chain relaxation appears to become single exponential with a long relaxation time which decreases as Φ_L decreases. One might explain this effect by dilation of the idealized tube of constraints due to polydispersity.[21] However, for the molecular weights used in these experiments, tube dilation is not expected to occur. Following the arguments of Doi et al.,[21] a reasonable criterion for ruling out tube dilation is

$$M_S^3/M_e^2M_L > 1$$

where M_e is the molecular weight between entanglements and M_i are the two component molecular weights, long and short. As mentioned in the Introduction, diffusion experiments support a somewhat more stringent requirement that $M_S^3/M_e^2M_L > 10$.[17] For the polymers used in this study, $M_S^3/M_e^2M_L > 100$. Therefore, the short polymer seems to be too long to cause a decrease in the longest relaxation time of the long chains by tube dilation. The rate of diffusion is not increased, but it appears to be more effective in allowing the long chains to relax in blends with $\Phi_L < 0.5$.

Another observation is that the addition of long chains to the matrix produces a significant retardation of the relaxation of the short chains. Observations on the diffusion coefficient of labeled chains into a matrix of different molecular weight have shown that the diffusion coefficient of shorter chains into a matrix of longer chains is independent of the molecular weight of the long-chain matrix.[17] Therefore, the reduction in the rate of relaxation of the short chains cannot be explained by a decrease in the rate of diffusive motion of the short chains. In light of eq 9, this prolonged relaxation may be due to a combination of anisotropy in the orientation of Rouse segments of the short chains and nematic orientation due to the surrounding matrix. A sustained anisotropy on the level of Rouse segments might arise if nematic orientation produces anisotropic diffusion of the short chains.[38] However, such an effect cannot be conclusively deduced from these results. An alternative analysis of the effect of nematic-like coupling on the relaxation of bidisperse melts is given in the Appendix. There we also present a method for determining the strength of nematic interaction from our measurements and apply it to our current results.

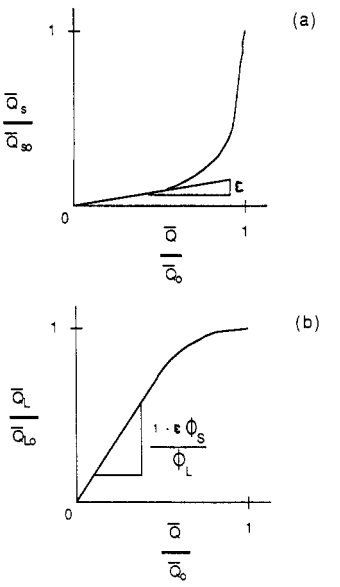

Figure 9. Schematic plots of component relaxation versus bulk relaxation for (a) the short chains and (b) the long chains which can be used to determine the nematic coupling parameter ϵ for a particular homopolymer system.

Acknowledgment. We are grateful to the National Science Foundation for support through the Presidential Young Investigator (G. Fuller) and Graduate Fellowship (J. Kornfield) programs. This work was also supported by the Exxon Foundation and the Center for Materials Reasearch at Stanford University. We thank Lewis Fetters for synthesizing the polymers employed in this study.

Appendix. Effect of Nematic Interaction on Polymer Melt Relaxation

The optical anisotropy of a polymer under stress arises at the level of the orientation distribution of chemical bonds along the chain; however, the stress arises from the entropic elasticity associated with statistical segments (Rouse segments or "bonds") composed of many chemical bonds. While it has been shown that the orientation distributions of bonds and of Rouse segments are proportional for the bulk, this may not be the case for each molecular weight component in a polydisperse melt. Considerable experimental research indicates that short-range orientational coupling (nematic interaction) acts between oriented polymer chains and surrounding free molecules, whether they are dissimilar penetrant probes or oligomers of the same polymer.[31-36] In addition, there is evidence that nematic interaction increases the bond level orientation in a dry rubber relative to that in a swollen rubber at a given level of stress.[50] The significance of this is that the enhancement in local orientation due to a short-range intermolecular coupling does not give an additional contribution to the stress. Further, experiments have shown that local orientation of free chains penetrating an extended network does not produce anisotropy in their radius of gyration.[51] Therefore, it is necessary to make a distinction between the local orientation on the scale of chemical bonds and that on the scale of statistical segments.[39]

The orientation of the chemical bonds may be described by the unit vectors $u_i(s)$, where s denotes the position of the bond along a chain and i denotes the vector component. For the purpose of defining a measure of nematic interaction, consider a polymer network or melt penetrated by a trace amount of oligomer. In the presence of nematic orientational coupling, a bulk state of orientation described by $\langle u_i u_j \rangle_{bulk}$ produces an orientational order in bonds belonging to a low molecular weight, dilute oligomer $\langle u_i u_j \rangle_{olig}$:

$$\langle u_i u_j \rangle_{olig} = \epsilon \langle u_i u_j \rangle_{bulk} \tag{A.1}$$

This defines the coupling parameter, ϵ, characteristic of the polymer species and state of the melt.

In an entangled melt, nematic-like interaction produces an increase in the orientational order of bonds relative to Rouse segments:

$$\left\langle u_i u_j - \frac{1}{3}\delta_{ij} \right\rangle = \frac{1}{1-\epsilon} \frac{3}{5n^2b^2} \left\langle r_i r_j - \frac{1}{3} r^2 \delta_{ij} \right\rangle \tag{A.2}$$

where the factor of $1/(1-\epsilon)$ describes the enhancement over that predicted by a gas-like theory of rubber elasticity. This alters eq 8 for the birefringence only in the value of the constant A. Applied to each component of a bidisperse system, however, the result of nematic orientation is a contribution to the orientation of bonds in K chains (long or short), which reflects the orientational order of the mean field surrounding a K chain. The orientation distribution of bonds in a K chain, $\langle u_i u_j \rangle_K$, has a contribution due to the orientation of Rouse segments along the K chain, $\langle r_i r_j \rangle_K$, and another due to nematic coupling to the orientation in the bulk, $\epsilon \langle u_i u_j \rangle$:

$$\left\langle u_i u_j - \frac{1}{3}\delta_{ij} \right\rangle_K = \frac{3}{5n^2b^2} \left(\left\langle r_i r_j - \frac{1}{3} r^2 \delta_{ij} \right\rangle_K + \frac{\epsilon}{1-\epsilon} \left\langle r_i r_j - \frac{1}{3} r^2 \delta_{ij} \right\rangle \right) \tag{A.3}$$

It is the orientation of bonds which gives rise to dichroism; therefore, in a system with K chains labeled we arrive at the result given in the introduction:

$$n_{ij}'' = C(\lambda) \left[\left\langle r_i r_j - \frac{1}{3} r^2 \delta_{ij} \right\rangle_K + \frac{\epsilon}{1-\epsilon} \left\langle r_i r_j - \frac{1}{3} r^2 \delta_{ij} \right\rangle \right] \tag{9}$$

Comparison of eq 8 and 9 shows the addition of a bulk Rouse segment orientation distribution term to the K chain dichroism.

Further analysis shows how the strength of the orientational coupling in a homopolymer melt can be determined from measurements of the bond level orientational relaxation of the long and short chains in a bidisperse melt. Following the notation of Doi et al.,[39] we define an order parameter tensor for K chains as

$$Q_{K,ij}(s,t) \equiv \frac{5a^2}{3b^2} \left\langle u_i u_j - \frac{1}{3}\delta_{ij} \right\rangle_K$$

which measures the orientation distribution of the bond at position s along the chain at time t, averaged over an ensemble of K chains. The average of $Q_{K,ij}(s,t)$ over the contour of a K chain gives the average order parameter of K chain bonds:

$$\bar{Q}_{K,ij} = \frac{1}{K} \int_0^K ds\, Q_{K,ij}(s,t)$$

After a sudden strain, the order in the melt is equal to $\bar{Q}_{O,ij}$. Furthermore, instantaneously, the order is molecular weight independent; therefore

$$\bar{Q}_{O,ij} = \bar{Q}_{SO,ij} = \bar{Q}_{LO,ij} \tag{A.4}$$

At every instant in time we have

$$\bar{Q}_{ij} = \Phi_S \bar{Q}_{S,ij} + \Phi_L \bar{Q}_{l,ij} \tag{A.5}$$

In the present experiments, the measured variables are $\bar{Q}_{ij}/\bar{Q}_{O,ij}$, $Q_{S,ij}/\bar{Q}_{SO,ij}$, and $\bar{Q}_{L,ij}/\bar{Q}_{LO,ij}$. Expressing eq A.5 in terms of the experimental observables gives

$$\frac{\bar{Q}_{ij}}{\bar{Q}_{O,ij}} = \Phi_S \frac{\bar{Q}_{SO,ij}}{\bar{Q}_{O,ij}} \frac{\bar{Q}_{S,ij}}{\bar{Q}_{SO,ij}} + \Phi_L \frac{\bar{Q}_{LO,ij}}{\bar{Q}_{O,ij}} \frac{\bar{Q}_{L,ij}}{\bar{Q}_{LO,ij}} \tag{A.6}$$

At times sufficiently long that a monodisperse melt of short chains would be fully relaxed, residual orientation of the short chains in a binary blend may be interpreted as resulting from a nematic-like orientation coupling

$$\frac{\bar{Q}_{S,ij}}{\bar{Q}_{SO,ij}} = \epsilon \frac{\bar{Q}_{ij}}{\bar{Q}_{O,ij}} \tag{A.7}$$

for $t \gg \tau S$, where ϵ is the usual coupling parameter. Therefore, a plot of $\bar{Q}_{S,ij}/\bar{Q}_{SO,ij}$ versus $\bar{Q}_{ij}/\bar{Q}_{o,ij}$ can be used to determine the coupling parameter ϵ, as shown in Figure 9. Under the same conditions, the long-chain relaxation is also proportional to the bulk relaxation:

$$\frac{\bar{Q}_{L,ij}}{\bar{Q}_{LO,ij}} = \frac{1-\epsilon\Phi_S}{\Phi_L} \frac{\bar{Q}_{ij}}{\bar{Q}_{O,ij}} \tag{A.8}$$

for $t \gg \tau_S$. A plot of $\bar{Q}_{L,ij}/\bar{Q}_{LO,ij}$ versus $\bar{Q}_{ij}/\bar{Q}_{O,ij}$ will have the general appearance shown in Figure 10 and provides an independent, although less sensitive, means to determine ϵ.

Work is in progress to obtain the short-chain relaxation at intermediate time, $\tau_S < t < \tau_L$, with sufficient accuracy to determine the coupling parameter ϵ for this polymer system, as defined in eq A.1. The method for determining ϵ described above indicates a value between 0.3 and 0.4 using the current results.

References and Notes

(1) Ninomiya, K.; Ferry, J. D. *J. Colloid Sci.* **1963**, *18*, 421.
(2) Masuda, T.; Kitagawa, K.; Inoue, T.; Onogi, S. *Macromolecules* **1970**, *2*, 116.
(3) Kurata, M.; Osaki, K.; Einaga, Y.; Sugie, T. *J. Polym. Sci., Polym. Phys. Ed.* **1974**, *12*, 849.
(4) de Gennes, P.-G. *J. Chem. Phys.* **1971**, *55*, 572.
(5) Doi, M.; Edwards, S. F. *J. Chem. Soc., Faraday Trans. 2* **1978**, *74*, 1789, 1802, 1818.
(6) Doi, M.; Edwards, S. F. *J. Chem. Soc., Faraday Trans. 2* **1979**, *75*, 32.
(7) Doi, M. *J. Polym. Sci., Polym. Phys. Ed.* **1980**, *18*, 1005, 2055.
(8) Graessley, W. W. *Adv. Polym. Sci.* **1982**, *47*, 67.
(9) Marrucci, M. *J. Polym. Sci., Polym. Phys. Ed.* **1985**, *23*, 159.
(10) Viovy, J. L. *J. Phys. (Les Ulis, Fr.)* **1985**, *46*, 847.
(11) Rubinstein, M.; Helfand, E.; Pearson, D. S. *Macromolecules* **1987**, *20*, 822.
(12) Montfort, J. P.; Marin, G.; Monge, D. *Macromolecules* **1984**, *17*, 1551.
(13) Watanabe, H.; Kotaka, T. *Macromolecules* **1984**, *17*, 2316.
(14) Watanabe, H.; Sakamoto, T.; Kotaka, T. *Macromolecules* **1985**, *18*, 1008, 1436.
(15) Struglinski, M. J.; Graessley, W. W. *Macromolecules* **1985**, *18*, 2630.
(16) Green, P. F.; Mills, P. J.; Palmstrom, C. J.; Mayer, J. W.; Kramer, E. J. *Phys. Rev. Lett.* **1984**, *53*, 2143.
(17) Green, P. F.; Kramer, E. J. *Macromolecules* **1986**, *19*, 1108.
(18) Antonietti, M.; Coutandin, J.; Sillescu, H. *Macromolecules* **1986**, *19*, 793.
(19) Tassin, J. F.; Monnerie, L. *J. Polym. Sci., Polym. Phys. Ed.* **1983**, *21*, 1981.
(20) Tassin, J. F.; Monnerie, L.; Fetters, L. J. *Polym. Bull. (Berlin)* **1986**, *15*, 165.
(21) Doi, M.; Graessley, W. W.; Helfand, E.; Pearson, D. S. *Macromolecules* **1987**, *20*, 1900.
(22) Noda, I.; Dowrey, A. E.; Marcott, C. *J. Polym. Sci., Polym. Lett. Ed.* **1983**, *21*, 99.

(23) Lefebvre, D.; Jasse, B.; Monnerie, L. *Polymer* **1983**, *24*, 1240.
(24) Lee, A.; Wool, R. P. *Macromolecules* **1986**, *19*, 1063.
(25) Lee, A.; Wool, R. P. *Macromolecules* **1987**, *20*, 1924.
(26) Bates, F. S.; Dierker, S. B.; Wignall, G. D. *Macromolecules* **1986**, *19*, 1938.
(27) Buckingham, A. D.; Hentschel, H. G. E. *J. Polym. Sci., Polym. Phys. Ed.* **1980**, *18*, 853.
(28) Doi, M.; Edwards, S. F. *The Theory of Polymer Dynamics*; Clarendon: Oxford, 1986.
(29) Doi, M. *J. Non-Newtonian Fluid Mech.* **1987**, *23*, 151.
(30) Kuhn, W.; Grün, F. *J. Polym. Sci.* **1946**, *1*, 183.
(31) Michl, J.; Thulstrup, E. W. *Spectroscopy with Polarized Light*; VCH: New York, 1986.
(32) Matsuoka, Y. *J. Phys. Chem.* **1980**, *84*, 1361.
(33) Schmidt, P.; Schneider, B. *Makromol. Chem.* **1983**, *184*, 2075.
(34) Jacobi, M. M.; Stadtler, R.; Gronski, W. *Macromolecules* **1986**, *19*, 2884.
(35) Sotta, P.; Deloche, B.; Herz, J.; Lapp, A.; Durand, D.; Rabadeux, J.-C. *Macromolecules* **1987**, *20*, 2769.
(36) Queslel, J.-P.; Erman, B.; Monnerie, L., to be submitted for publication.
(37) Jarry, J.-P.; Monnerie, L. *Macromolecules* **1979**, *12*, 316.
(38) Merrill, W. W.; Tirrell, M., to be submitted for publication.
(39) Doi, M.; Pearson, D. S.; Kornfield, J.; Fuller, G. G., to be submitted for publication.
(40) Johnson, S. J.; Frattini, P. L.; Fuller, G. G. *J. Colloid Interface Sci.* **1985**, *104*, 440.
(41) Lodge, A. S.; Meissner, J. *Rheol. Acta* **1972**, *11*, 351.
(42) Osaki, K.; Kimura, S.; Kurata, M. *J. Polym. Sci., Polym. Phys. Ed.* **1981**, *19*, 517.
(43) Leonov, A. I. *Rheol. Acta* **1976**, *15*, 85.
(44) Azzam, R. M. A.; Bashara, N. M. *Ellipsometry and Polarized Light*, North-Holland: Amsterdam, The Netherlands, 1987.
(45) Morton, M.; Fetters, L. J. *Rubber Chem. Technol.* **1975**, *48*, 359.
(46) Rachapudy, H.; Smith, G. G.; Raju, V. R.; Graessley, W. W.; *J. Polym. Sci., Polym. Phys. Ed.* **1979**, *17*, 1211.
(47) Pearson, D. S.; Kiss, A. D.; Kornfield, J. A.; Fuller, G. G., to be submitted for publication.
(48) Laun, H. M. *Rheol. Acta* **1978**, *17*, 1.
(49) Pearson, D. S.; Rochefort, W. E. *J. Polym. Sci., Polym. Phys. Ed.* **1982**, *20*, 83.
(50) Fukuda, M.; Wilkes, G. L.; Stein, R. S. *J. Polym. Sci., Polym. Phys. Ed.* **1971**, *9*, 1417.
(51) Bouë, F.; Farnoux, B.; Bastide, J.; Lapp, A.; Herz, J.; Picot, Cl. **1986**, *1*, 637.

Local Segmental Dynamics of Polyisoprene in Dilute Solution: Solvent and Molecular Weight Effects

Dean A. Waldow, Brian S. Johnson, Patrick D. Hyde, and M. D. Ediger*

Department of Chemistry, University of Wisconsin, Madison, Wisconsin 53706

Toshiaki Kitano† and Koichi Ito

Department of Materials Science, Toyohashi University of Technology, Toyohashi 440, Japan. *Received June 14, 1988; Revised Manuscript Received August 19, 1988*

ABSTRACT: A picosecond holographic grating technique has been utilized to observe the solvent and molecular weight dependence of the local segmental dynamics of anthracene-labeled polyisoprene in dilute solution. Solvent quality influences the local dynamics by changing the local segment concentration in the vicinity of the labeled segment. The local dynamics in a Θ solvent exhibited a molecular weight dependence not observed in good solvents. The shape of the orientation autocorrelation function was constant under all conditions investigated. These results are consistent with the hypothesis that local segmental dynamics in dilute solution depend only upon solvent viscosity and solvent thermodynamic power.

I. Introduction

The local segmental dynamics of polymer chains have a strong influence on the macroscopic properties of polymeric systems. In polymer solutions where local dynamics occur on picosecond and nanosecond time scales, this influence is mainly through the larger distance scale motions which dominate ordinary viscoelastic properties under these conditions. Because dynamics on the length scale of a few monomer units are strongly dependent upon the details of the monomer structure, information about local segmental dynamics provides an important intermediate link between molecular structure and larger motions. In a polymer melt near T_g, the time scales for local conformational transitions slow dramatically. It is widely held that the quenching of backbone conformational transitions is intimately connected with the glass transition. Certain types of local segmental dynamics can also directly influence material properties in the sub-T_g region. Given the fundamental significance of local segmental dynamics, it is not surprising that a wide variety of experimental techniques have been utilized in their investigation in recent years. Among these are dielectric relaxation,[1] NMR,[2] dynamic light scattering,[3] ESR,[4] and optical spectroscopic techniques.[5-13]

In every experimental measurement of local segmental dynamics, both the molecular structure of the polymer and the environment of the chains contribute to the observed dynamics. The contribution of the environment must be thoroughly understood before progress can be made on the question of how the structure influences the dynamics. One question of particular interest is the extent to which the local chemical details of solvent–polymer interactions must be considered. Since local segmental dynamics occur on about the same length scale as the dimensions of solvent molecules, it is not obvious that the effect of the solvent on the local dynamics will be adequately described by bulk properties. Indeed, the reorientation of small solute molecules even in simple solvents is known to be strongly influenced by solvent–solute interactions.[14]

In this paper we focus our attention on the influence of solvent, temperature, and molecular weight on the local segmental dynamics of polyisoprene in dilute solution. A transient holographic grating technique was utilized to observe the orientation autocorrelation function of a backbone bond in anthracene-labeled polyisoprene. The anthracene chromophore was covalently bonded into the chain such that the transition dipole for the lowest electronic excited state lies along the chain backbone. This

† Current address: Polyplastics Co., Ltd., 973 Miyajima, Fuji-City, Shizuoka-Pref. 416, Japan.

0024-9297/89/2222-1345$01.50/0